

Real-time Orthorectified Visualization of Aerial Remote Sensing Images

Ying Yang,¹ Xi Zhai,^{1*} and Fengzhu Liu^{2**}

¹National Geomatics Center of China,
No. 28 Lianhuachi West Road, Haidian District, Beijing 100830, China

²Beijing Institute of Surveying and Mapping,
No. 15, Yangfangdian Road, Haidian District, Beijing 100038, China

(Received July 10, 2024; accepted August 16, 2024)

Keywords: remote sensing, orthorectified visualization, Voronoi polygon, high-performance computing, emergency response

In this article, we address the practical needs for the rapid processing and application of aerial photogrammetry remote sensing images, proposing a method based on high-performance computing technology to achieve the real-time, dynamic orthorectified visualization of aerial remote sensing images. This method differs from traditional orthorectification processing and application workflows, utilizing high-performance parallel computing capabilities to directly achieve orthorectification based on raw aerial images. In this paper, we also compare and analyze four different real-time orthorectified visualization schemes to meet various application needs, evaluating the efficiency and accuracy of the proposed method. Finally, experimental results with unmanned aerial vehicle (UAV) flight image data indicate that this method is feasible, with real-time computational results meeting practical application requirements in terms of effect and performance.

1. Introduction

Over the past decade, aerial photography technology has rapidly developed. In particular, the application of unmanned aerial vehicle (UAV) remote sensing technology has attracted increasing attention and has been widely used in aerial photography measurement, geographic monitoring, emergency rescue and disaster reduction, agricultural remote sensing surveys, and so forth.⁽¹⁾ The UAV remote sensing system has filled the gap in the low-altitude region between traditional remote sensing platforms from ground to space.⁽²⁾ The research and development of hardware systems for UAV remote sensing has achieved numerous successes, and software development has also yielded fruitful outcomes, highlighted by the emergence of commercial software such as Inpho, Context Capture, Bingo ATM, LPS,⁽³⁾ Pix4D, and GTA 3D modeling software. China also has achieved significant advancements in UAV surveying systems, with a range of UAV systems for surveying and mapping now available in the market. There have been

*Corresponding author: e-mail: zhaixi@ngcc.cn

**Corresponding author: e-mail: 540508818@qq.com

<https://doi.org/10.18494/SAM5233>

numerous research accomplishments in software development, such as Pixel Grid and the Map-AT aerial survey processing system,⁽⁴⁾ as well as the DP Grid aerial photogrammetry system.⁽⁵⁾

Existing research on rapid processing methods for aerial remote sensing images primarily targets key technical processes in aerial triangulation, geometric correction, and stitching, such as panoramic image stitching, direct geometric correction stitching based on ground control points, image space projection transformation stitching based on image tie points, and stitching methods based on aerial triangulation and orthorectification.^(6–15) Zhang *et al.* introduced a video stitching method based on the homography matrix,⁽⁸⁾ and Xie *et al.* introduced a technical method for multicamera image stitching with tie points from image matching,⁽⁹⁾ and both are similar to the method of image space projection transformation stitching. Zhang provided an overview of the current status of rapid UAV image stitching and analyzed the differences between the methods and pointed out that different methods are suitable for different applications.⁽¹⁵⁾ All of these methods necessitate a sequence of processing steps to obtain processed image file results from the original image, which cannot be achieved in real time.

From the analysis of existing data processing procedures, a real-time orthorectified method for aerial photography remote sensing images using a graphics processing unit (GPU) for high-performance computing is proposed to revolutionize traditional data processing workflows. The method advocates the direct use of raw data and aerial triangulation results, even high-precision original flight global navigation satellite system (GNSS) and inertial measurement unit (IMU) data, to achieve real-time, dynamic, orthorectified visualization applications for aerial photography remote sensing image data.

2. Workflow for Aerial Image Data Processing

2.1 Traditional data processing workflow

To generate a comprehensive orthoimage from raw data, several steps need to be taken. These include data preprocessing, image distortion correction, flight line data editing and organization, the establishment of a 3D data processing project, the automatic extraction of connected points within each flight strip, the extraction of points between flight strips, relative orientation, the annotation of control points, absolute orientation, automatic dense point matching and filtering to derive a digital elevation model (DEM), automatic orthorectification based on a single image, editing digital orthophoto map (DOM) image stitching lines, radiometric and color correction, and the output of stitched images.

The essential steps in the image processing workflow, such as distortion correction, format conversion, tie point extraction, automatic relative and absolute orientation, DEM extraction, DOM correction, and mosaic, consume a considerable amount of time, which severely hampers the timeliness of UAV systems in emergency response and disaster relief. The detailed data processing workflow is shown in Fig. 1.

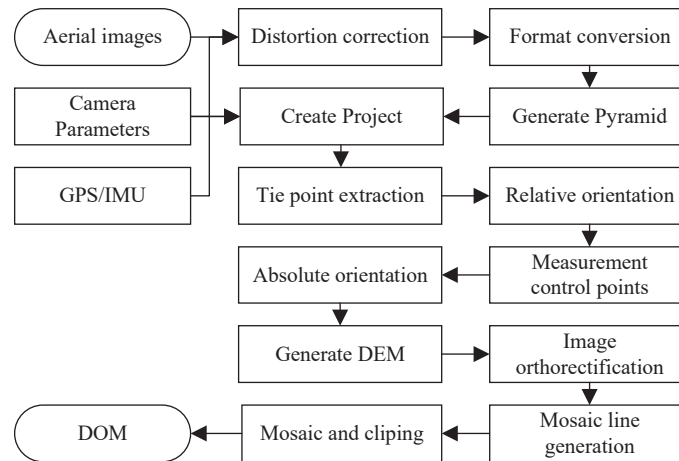


Fig. 1. Traditional data processing workflow.

2.2 Real-time orthorectified visualization solutions

In this work, we simplify the data processing of aerial photogrammetry images, improve two processes of image processing and application implementation, propose four feasible data visualization schemes, and enhance the timeliness of aerial photography remote sensing system data processing and application. The four orthorectified visualization schemes are listed below.

- (1) Orthorectified visualization with GPS/IMU data and raw images
- (2) Orthorectified visualization with relative orientation results of images
- (3) Orthorectified visualization with absolute orientation results of images
- (4) Orthorectified visualization with absolute orientation and DEM products of images

The workflow diagram of the data processing system is shown in Fig. 2.

Traditional orthorectification algorithms such as digital differential rectification are achieved through collinearity conditions, utilizing collinearity equations to convert ground grid points to pixel coordinates, calculating pixel coordinates based on ground coordinates and elevation at the target resolution grid, and interpolating to obtain image color values for rectification. The proposed rapid visualization method for UAV images involves GPU acceleration and Voronoi diagram indexing for multiscale texture real-time scheduling updates. It accomplishes coordinate projection through the image grid, utilizes GPU acceleration for texture resampling, and integrates the Voronoi diagram for multiscale texture optimization. In practical applications, visualization schemes and image grid coordinate projection methods are chosen on the basis of data application requirements. The transformation from image coordinates to ground coordinates can be achieved through two methods: using the average terrain height in the survey area and DEM. The first approach in these methods utilizes the average terrain height in the survey area for image grid coordinate projection (Approach 1), whereas the remaining three approaches use DEM data. Ground coordinates solved by connecting points obtained through relative orientation adjustment can be used to fit coarse DEM data (Approach 2). Additionally, after absolute orientation, coarse DEM grid data can be obtained by fitting oriented points and control point

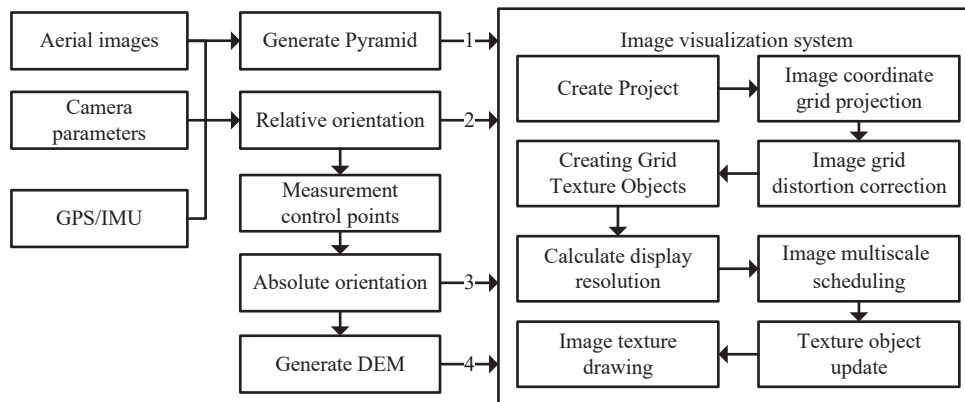


Fig. 2. UAV image real-time orthographic visualization flow chart.

coordinates (Approach 3). Alternatively, DSM can be generated through dense point matching to improve DEM accuracy (Approach 4).

3. Principle of Algorithm

3.1 Image grid ground coordinate projection

The main idea of the real-time image orthorectified visualization proposed in this paper involves using the collinearity condition equation to project the ground coordinates of the image grid, and then employing the texture resampling technique of the GPU to achieve real-time image orthorectified visualization. The key processing involves the projection transformation from image coordinates to ground coordinates, achieving the mapping between texture and ground coordinates, and completing the texture unit orthorectified visualization mapping. The transformation from image coordinates to ground coordinates can be calculated using the average terrain height or DEM data.

3.1.1 Projection of image grid ground coordinates based on average terrain height

Imagery is organized in a pyramid and tile data format; thus, the image grid is consistent with the image's underlying tile structure, using the same dimensions and sizes. This ensures that texture data blocks are consistent with the imagery's tile organization structure, facilitating the scheduling of image data.

The image grid point coordinates for their corresponding ground points are calculated with the collinearity condition equation. The method presented in this paper takes into account the correction of camera image distortions, with the collinearity condition equation considering distortion correction as follows.⁽¹⁶⁾

$$\begin{cases} x - x_0 + \Delta x = -f \frac{a_1(X - X_s) + b_1(Y - Y_s) + c_1(Z - Z_s)}{a_2(X - X_s) + b_2(Y - Y_s) + c_2(Z - Z_s)} \\ y - y_0 + \Delta y = -f \frac{a_3(X - X_s) + b_3(Y - Y_s) + c_3(Z - Z_s)}{a_2(X - X_s) + b_2(Y - Y_s) + c_2(Z - Z_s)} \end{cases} \quad (1)$$

Here, Δx and Δy are the correction values for distortions in the grid point's image coordinates; x and y denote the grid's image coordinates; x_0 and y_0 correspond to the image coordinates of the principal point; f represents the focal length. X, Y, Z and X_s, Y_s, Z_s respectively signify the ground coordinates associated with the image point and the coordinates of the imagery's projection center. The elements $a_1, a_2, a_3, b_1, b_2, b_3, c_1, c_2,$ and c_3 constitute the rotation matrix derived from the attitude angles.

The terms $(\Delta x, \Delta y)$ are based on the classical nonlinear distortion model for digital camera systems,^(17,18) with the formula given below.

$$\begin{aligned} \Delta x &= \bar{x}(k_1 r^2 + k_2 r^4 + k_3 r^6) + p_1(2\bar{x}^2 + r^2) + 2p_2\bar{x}\bar{y} + b_1\bar{x} + b_2\bar{y} \\ \Delta y &= \bar{y}(k_1 r^2 + k_2 r^4 + k_3 r^6) + 2p_1\bar{x}\bar{y} + p_2(2\bar{y}^2 + r^2) \end{aligned} \quad (2)$$

Here, \bar{x} and \bar{y} are the coordinates of the distorted image points in the original imagery, $r = \sqrt{\bar{x}^2 + \bar{y}^2}$. Utilizing the image point coordinates (x, y) at the grid points, the image's exterior orientation components (X_s, Y_s, Z_s) , camera parameters $(x_0, y_0, f, k_1, k_2, p_1, p_2, b_1, b_2)$, and the mean ground height of the survey area (the mean ground height Z of the image), one can compute the ground coordinates (X, Y) where the grid points are projected, as detailed in the following process. The ground coordinate formula is derived from the collinearity equation as⁽¹⁹⁾

$$\begin{aligned} \frac{(X - X_s)}{(Z - Z_s)} &= \frac{a_1 x + a_2 y - a_3 f}{c_1 x + c_2 y - c_3 f}, \\ \frac{(Y - Y_s)}{(Z - Z_s)} &= \frac{b_1 x + b_2 y - b_3 f}{c_1 x + c_2 y - c_3 f}. \end{aligned} \quad (3)$$

The solution of the equation yields the values of (X, Y) as

$$\begin{aligned} X &= \frac{(a_1 x + a_2 y - a_3 f) * (Z - Z_s)}{c_1 x + c_2 y - c_3 f} + X_s, \\ Y &= \frac{(b_1 x + b_2 y - b_3 f) * (Z - Z_s)}{(c_1 x + c_2 y - c_3 f)} + Y_s. \end{aligned} \quad (4)$$

3.1.2 Projection of image grid ground coordinates based on DEM

The principle of projecting image grid ground coordinates based on DEM is consistent with the previously mentioned coordinate projection based on average terrain height, which involves solving using collinearity condition equations. The main difference lies in the need to intersect a line with the terrain to achieve the projected coordinates, with the challenge being the varying terrain relief, which does not allow for an efficient and rapid determination of the intersection with the terrain grid. To address this issue, we employed an iterative approximation method to rapidly calculate the projected coordinates. Using the interior and exterior orientation elements of the image, the coordinates of the image points, we calculated the vector of the light ray composed of the photographic center and image points using the following formula:

$$\begin{bmatrix} X \\ Y \\ Z \end{bmatrix} = R * \begin{bmatrix} x - x_0 + \Delta x \\ x - x_0 + \Delta x \\ -f \end{bmatrix} = \begin{bmatrix} a_1 & a_2 & a_3 \\ b_1 & b_2 & b_3 \\ c_1 & c_2 & c_3 \end{bmatrix} * \begin{bmatrix} x - x_0 + \Delta x \\ x - x_0 + \Delta x \\ -f \end{bmatrix}. \tag{5}$$

Here, R represents the rotation matrix composed of exterior orientation elements. We obtained the ray vector and then used the elevation solving algorithm to iteratively solve the intersection of the line and terrain. The flowchart of the solution process is shown in Fig. 3.

3.2 Real-time orthorectification of images with texture resampling

The digital differential rectification algorithm (indirect method) utilizes point-by-point interpolation methods, such as bilinear interpolation and cubic convolution. Initially, the elevation is interpolated within DEM data using the planar coordinates of the orthoimage pixels, followed by the determination of the corresponding image point coordinates using the collinearity condition equations, and finally obtaining the grayscale values through the image

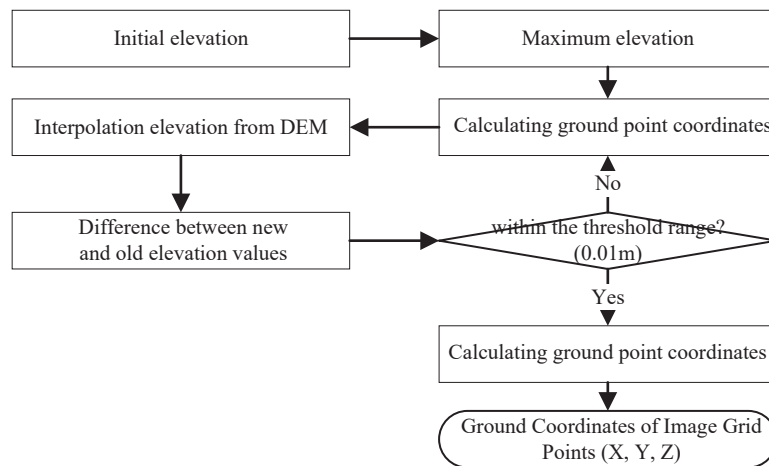


Fig. 3. Flowchart for calculating the ground coordinates of image grid points.

interpolation algorithm of the digital image. Calculating the image grayscale values point by point requires substantial computational time and must be performed for each image, which is inefficient and cannot meet the requirements for real-time display. In this work, we employed a texture resampling algorithm to realize the aforementioned algorithm in real time. Image grid coordinate projection [as shown in Fig. 4(a)] and texture resampling [as shown in Fig. 4(b)] are used to perform the interpolation of terrain data and the resampling of the image. A terrain triangulation network is constructed using the ground projection coordinates of the image grid, and terrain texture correction is completed through plane fitting and bilinear interpolation. Grid data are used to construct a terrain triangulation network (as shown in Fig. 4), where the 3D geographical coordinates of each vertex on the triangulation network correspond to the ground 3D coordinates of the image point, allowing for the acquisition of the image texture coordinates of the three vertices on the triangular surface. Subsequently, a linear interpolation algorithm is employed to map the textures of the triangulation network, a task accomplished using the texturing capabilities of GPU hardware. Compared with traditional per-pixel digital differential rectification, efficiency is considerably enhanced, allowing for the real-time correction and display of images. The texture resampling method reveals that the size of the triangulation network affects the geometric precision of the visualization, with the terrain constructed by the triangulation network being a fit to high-precision DEM data. When the size of the triangulation network approximates that of the DEM data, the accuracy of the triangulation network increasingly aligns with that of the DEM data, and the geometric precision of the visualization similarly approaches that of the orthoimage. Achieving dynamic orthoimage visualization across various scales is an important theoretical basis for realizing real-time visualization in this paper.

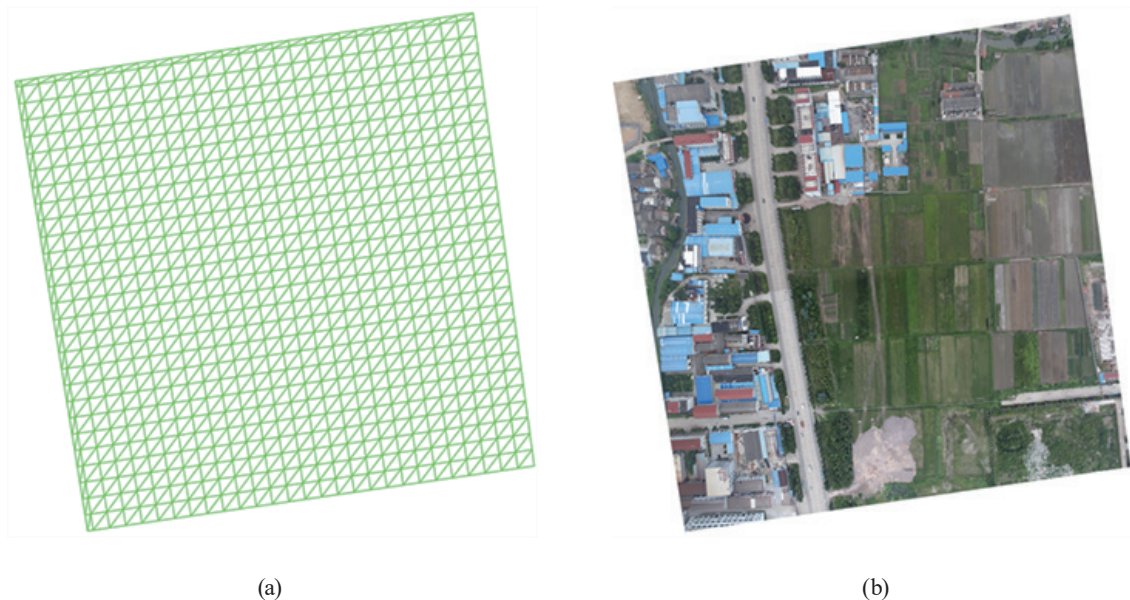


Fig. 4. (Color online) (a) Image grid and (b) texture of image grid coordinate projection.

3.3 Optimization of texture multiscale dynamic updating based on Voronoi diagrams

Ensuring the priority use of high-quality textures, saving texture data scheduling time, and improving real-time image visualization efficiency are important considerations. The dynamic scheduling of multiscale texture images is also essential for achieving real-time orthorectification. In this study, we used grid indexing and Voronoi diagrams to achieve the efficient dynamic scheduling and updating of data. The Voronoi polygon, also known as the Thiessen polygon, is formed by the perpendicular bisectors of each polygon center and its neighboring centers. The Voronoi diagram of the image area is constructed using the ground nadir point of each image as the center in this paper. The ground nadir point is closest to the photography center, resulting in higher image resolution and quality.

As shown in Fig. 5, the Voronoi diagram based on the ground nadir point is distributed in the relatively central position of the image. Consequently, choosing the ground nadir point as the center of the Voronoi diagram can prioritize the insertion of high-quality image textures, reduce the likelihood of image edge distortion and the usage of blurry textures, and ensure high-quality image texture visualization. Additionally, by using Voronoi diagrams for indexing, only texture

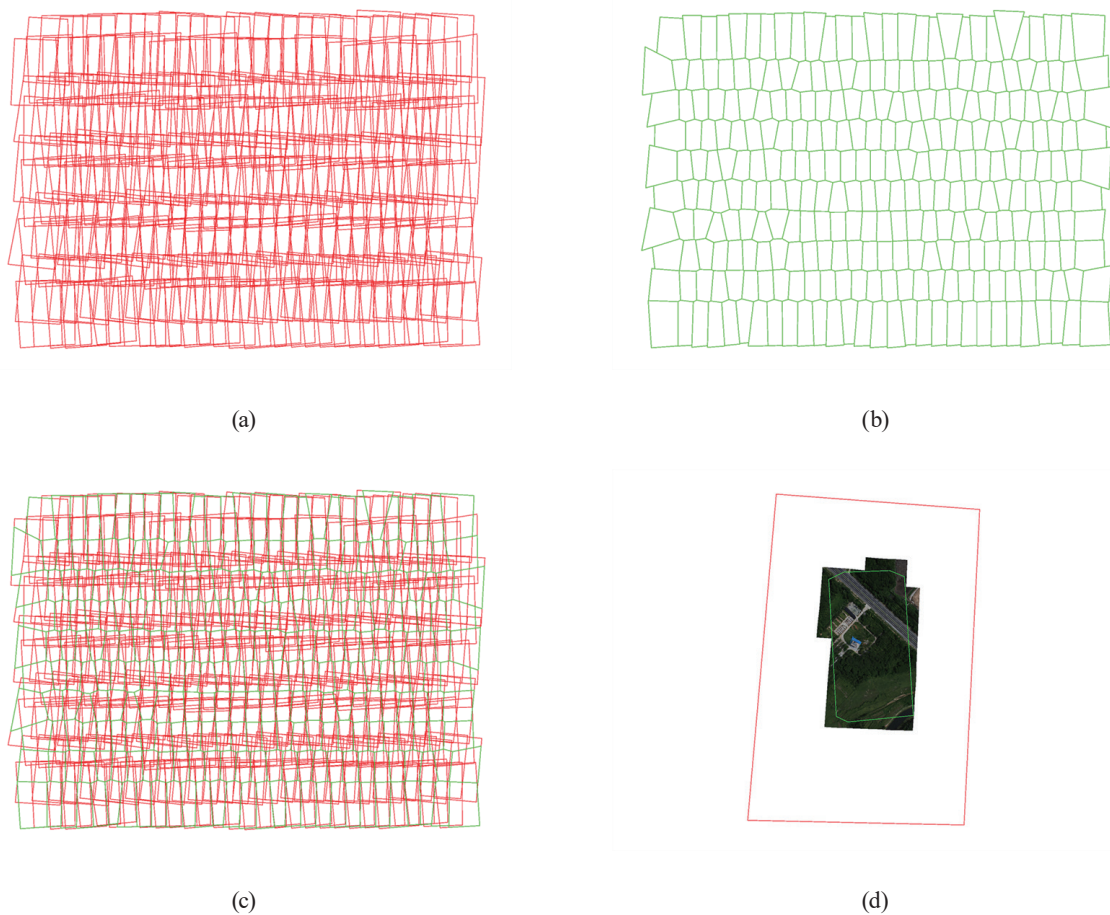


Fig. 5. (Color online) (a) Image bounds, (b) Voronoi schematic of images, (c) spatial relationship between the image bounds and the Voronoi polygon, and (d) single image schematic.

blocks that intersect with the Voronoi diagram are scheduled for very image. In comparison with the entire image, the area scheduled for image updates is significantly reduced, thereby doubling the efficiency of image texture updates. This is crucial for enhancing real-time multiscale updates of low-altitude images with large overlaps.

Multiscale texture updates are dynamically adjusted on the basis of the visual viewport range and resolution parameters. On the basis of the viewport resolution parameters, combined with the image resolution parameters and pyramid information, we confirm the optimal pyramid layer for visualization. Subsequently, we complete the scheduling of texture data on the basis of the pyramid parameters and terrain grid data. The advantage of scheduling different scale image data is that the number of pyramid data blocks that need to be accessed for images at different scales is consistent. This scheduling method significantly enhances the user experience of image roaming. The specific process diagram is shown in Fig. 6.

4 Experiment and Results

4.1 Experimental dataset

The dataset used in this experiment was acquired using a small fixed-wing UAV aerial photography system. The system was equipped with a GPS/IMU measurement system and used a Canon 5D Mark II digital SLR camera with a fixed focal length of 24.4621 mm. The image format is 5616×3744 pixels (each pixel is approximately $6.4 \mu\text{m}$ on the sensor). The survey area was covered by 10 flight lines, resulting in a successful acquisition of 546 aerial images. The within-flight-line overlap was 80%, and the between-flight-line overlap was 50%. The terrain

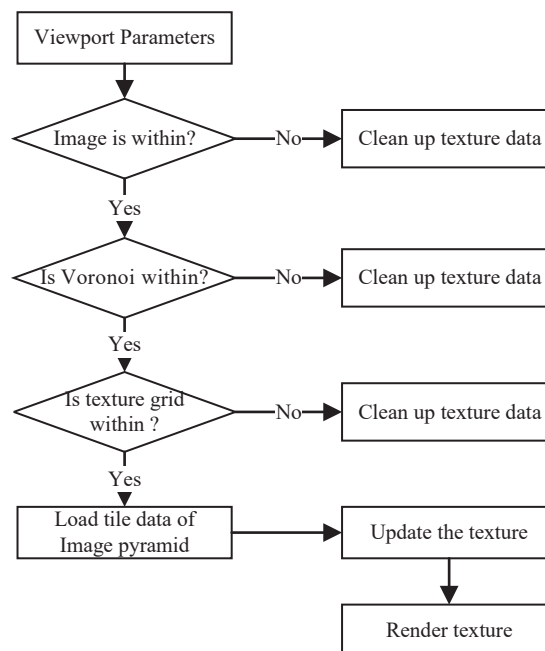


Fig. 6. Image texture update and display based on GPU and image pyramid.

elevation varied from 100 to 150 m, with an average elevation of 130 m. The flight was conducted at a relative altitude of 500 m.

The computer configuration used for testing is as follows: a Dell Precision 5520 laptop with a Microsoft Windows 10 x64 operating system and a display resolution of 1920*1080 pixels. The CPU is an Intel Core I7-7820HQ with 32 GB of RAM and 2 TB NVME SSD; the GPU is an NVIDIA M1200 with 4 GB of graphics memory.

4.2 Results and discussion

The method presented in this paper is implemented through four visualization schemes using various terrain data for real-time orthographic visualization. The overall visualization effect of the experimental data is illustrated in Fig. 7.

To further compare and analyze the differences in the visualization effects of different schemes, we also present the partial visualization effects of four different terrain data, namely, roads, buildings, flat terrain, and hilly terrain, as shown in Figs. 8–11, respectively.

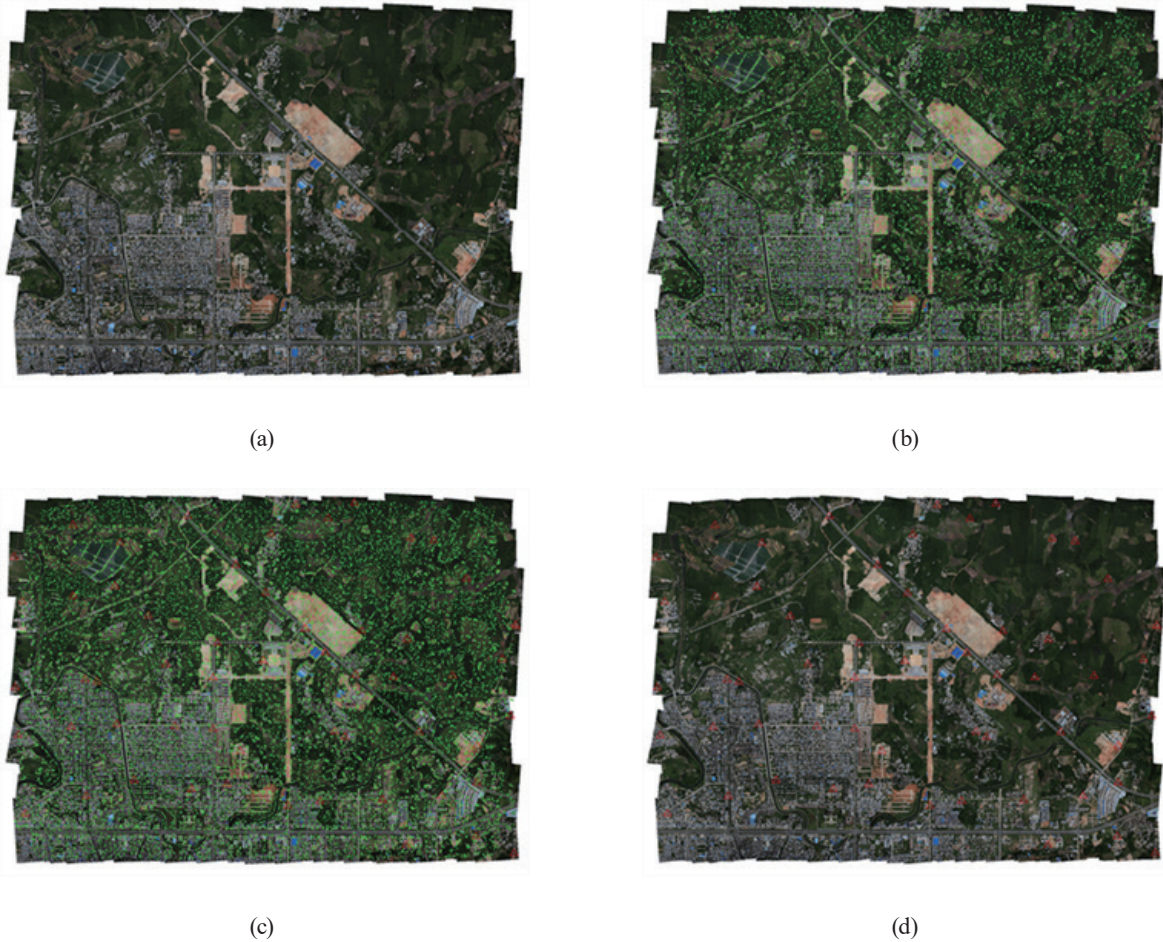


Fig. 7. (Color online) (a) Based on GNSS/IMU and average terrain height, (b) based on relative orientation results, (c) based on absolute orientation results, and (d) based on absolute orientation results and DEM data.

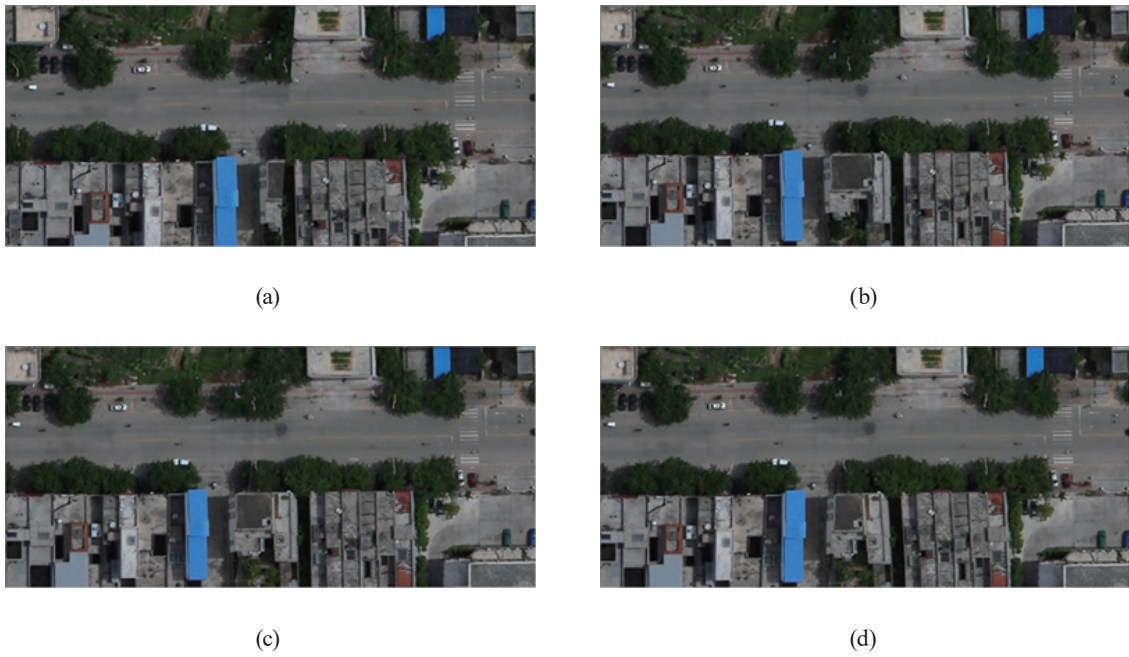


Fig. 8. (Color online) (a) Scheme 1, (b) Scheme 2, (c) Scheme 3, and (d) Scheme 4 for roads.

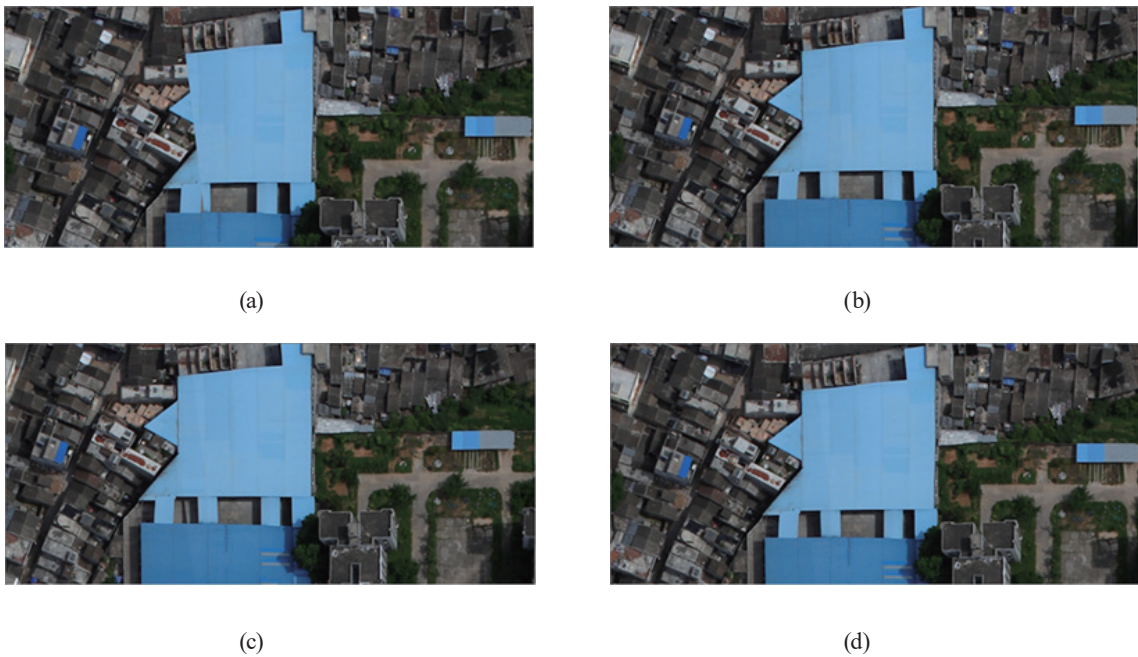


Fig. 9. (Color online) (a) Scheme 1, (b) Scheme 2, (c) Scheme 3, and (d) Scheme 4 for buildings.

Figure 7 demonstrates that the real-time orthorectified visualization methods based on GPU and Voronoi diagrams, implemented through different approaches, all achieve effective image stitching, meeting the needs of emergency services. By observing the overall experimental

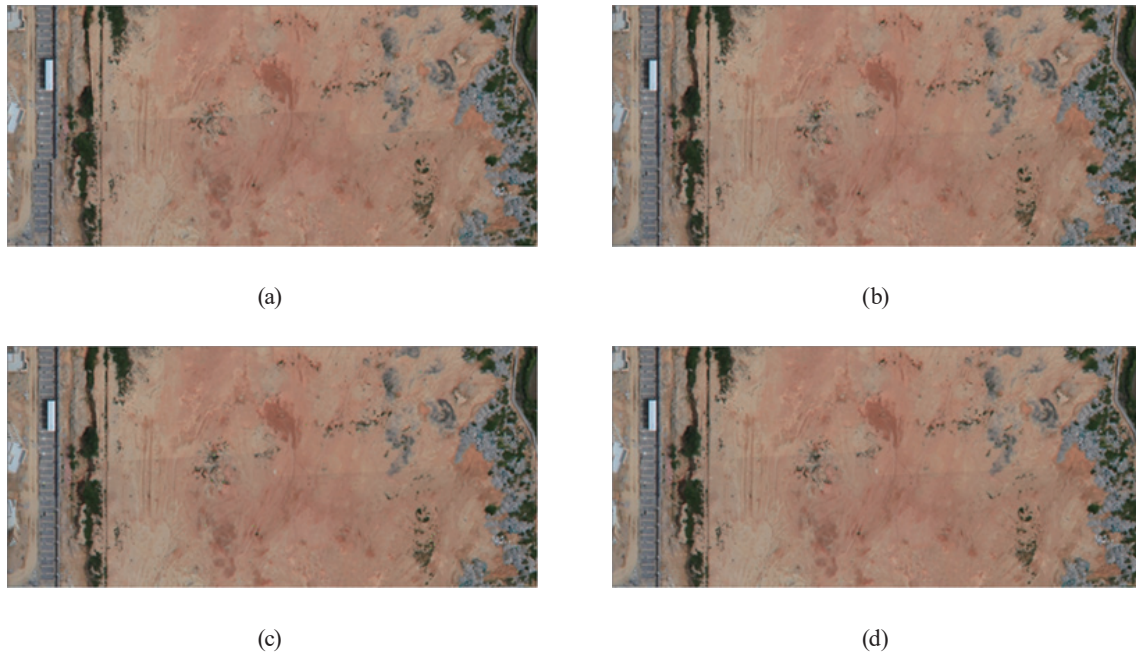


Fig. 10. (Color online) (a) Scheme 1, (b) Scheme 2, (c) Scheme 3, and (d) Scheme 4 for flat terrain.

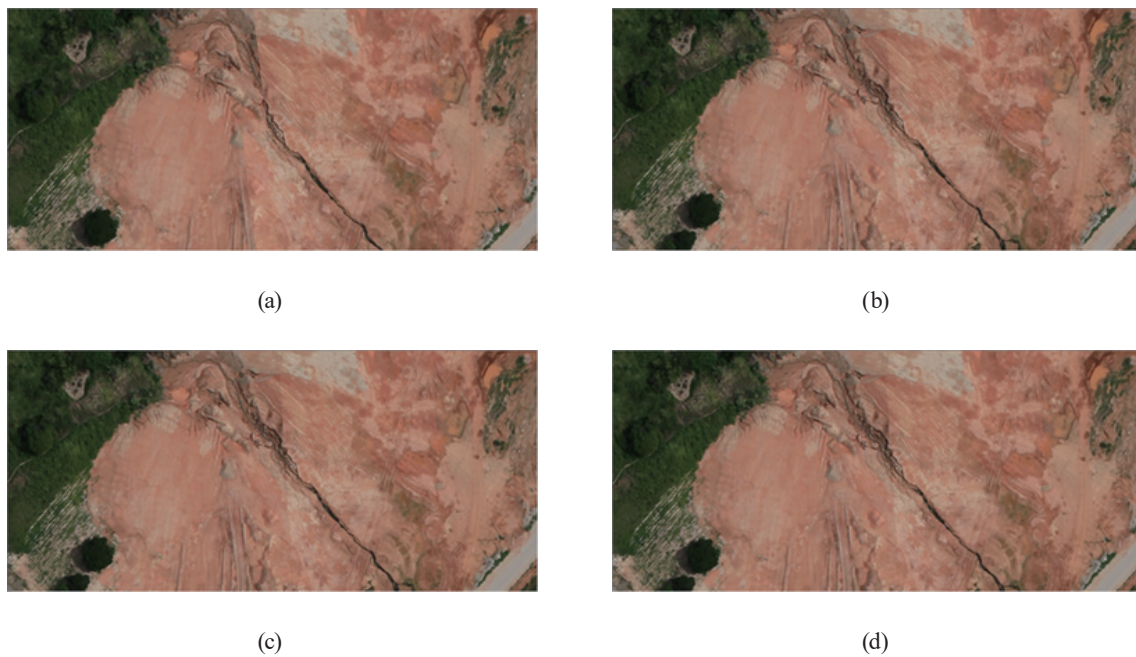


Fig. 11. (Color online) (a) Scheme 1, (b) Scheme 2, (c) Scheme 3, and (d) Scheme 4 for hilly terrain.

results of the visualization roaming images based on GPS and IMU data [as shown in Fig. 7(a)], this approach exhibits greater stitching errors than the other three schemes. When zoomed in on details, the misalignment at the image edges becomes distinctly visible. For instance, a continuous road depicted in the image suffers from discontinuity in its overall display owing to

constantly changing elevation, resulting in misalignment, with higher consistency within a single flight strip and lower consistency between different strips. However, this approach does not require image tie point matching or DEM data to grasp the overall situation of the survey area, which is of significant importance for applications involving drone emergency disaster relief. The overall integration effect of the visualization roaming images based on GPS and IMU data is entirely dependent on the accuracy of the GPS and IMU systems, with system precision having a notable impact on orthographic projection errors. For the aerial survey systems equipped with high-precision GPS and IMU systems and a stable platform, this approach tends to have an advantage in practical applications.

The image visualization effect based on relative orientation results [Fig. 7(b)] reveals that fitting the terrain model using the points information computed from tie points in relative orientation results can effectively mitigate stitching misalignment caused by the average terrain height model. As shown in Figs. 8–11, in areas with flat terrain (roads and grasslands), the terrain model obtained through the interpolation of object points can better compensate for stitching gaps caused by terrain, and the orientation enables the acquisition of more accurate external orientation elements of images, achieving excellent stitching display results in the flat terrain region. However, in areas with complex terrain, such as the buildings shown in Fig. 9, the terrain in the building areas is elevated owing to the effect of tie points on the buildings, resulting in the final outcome of projection distortion of the buildings.

The image orthorectified visualization effect based on different types of DEM data [Fig. 7(b, c, d)] shows a significant improvement in accuracy compared with that based on average terrain height [Fig. 7(a)]. As demonstrated in Figs. 8–11, in areas where the terrain is flat (roads and flat area), there is no significant difference between the visualization effects based on DEM data and the terrain model fitted from the absolute orientation result, indicating that the interpolated DEM data can effectively compensate for the inconsistencies in stitching caused by terrain variations.

4.3 Performance analysis

The method described in this paper does not differ in the data processing workflow but employs an image visualization technique that diverges from the traditional mode of image rectification, uniform lighting, and mosaicking to output orthoimages, directly utilizing raw image data, combined with orientation results, to achieve orthorectified visualization. To analyze the efficiency and performance of this method, we divided the entire real-time data processing workflow into eight steps as follows: (1) importing the project file, (2) extracting pyramid parameters, (3) projecting the average height terrain grid, (4) projecting the DEM data terrain grid, (5) rendering the complete image, (6) zooming in the view, (7) zooming out the view, and (8) moving the view. It also statistically analyzes the algorithm's runtime efficiency based on GPU acceleration and CPU single threading, GPU and CPU multithreading, and optimization using Voronoi diagrams. Table 1 provides detailed statistical results, where the operations for image roaming are all quantified at the same scale and extent of operation (with a zoom ratio of $1\times$ and a movement distance of half the view size).

Table 1
Statistical results of efficiency (units: s).

Method	STEP 1	STEP 2	STEP 3	STEP 4	STEP 5	STEP 6	STEP 7	STEP 8
Single-threaded	0.770	36.785	3.679	18.620	8.796	3.780	2.870	2.748
Multithreaded	0.783	5.967	0.979	3.124	1.997	0.952	0.788	0.421
Voronoi-optimized	0.779	5.952	0.976	3.116	0.379	0.166	0.152	0.096

The results in Table 1 show that the first four steps primarily involve data preparation operations, and the process based on multithreading scheduling is significantly faster than traditional single-threaded processing, particularly for map projection calculations where the advantage of multithreading is evident. In the latter four steps, which mainly involve texture update operations, the performance of texture multiscale optimization based on Voronoi diagrams has been improved considerably.

5. Conclusions

In this paper, we addressed and enhanced a time-consuming process in traditional aerial photogrammetry remote sensing image processing workflows by proposing a multiscale real-time texture image scheduling method. This method leverages GPU technology combined with Voronoi diagram indexing to achieve the real-time orthorectified visualization of aerial photogrammetry imagery. This method employs real-time computational rendering technology to replace traditional orthorectification processes, directly displaying orthorectified images from raw aerial imagery data. By substituting the central projection model in the algorithm with the rational polynomial coefficients model, this method can also be applied to the real-time orthorectified visualization of satellite remote sensing imagery, based on its core algorithm principles. The key contribution of this method lies in its use of high-performance real-time computing technology to achieve critical processes in traditional photogrammetric data processing. Directly implementing orthorectification and visualization using raw image data has significant implications for remote sensing applications based on high-performance computing and AI neural networks.

Acknowledgments

The authors would like to express their gratitude to the editors and reviewers for their constructive and helpful comments for the substantial improvement of this paper. This work is supported in part by the National Natural Science Foundation of China General Project (62076027).

References

- 1 J. Sun, Z. J. Lin, and H. X. Cui: *Remote Sens. Inf.* **26** (2003) 48 (in Chinese). <https://doi.org/10.3969/j.issn.1000-3177.2003.01.014>
- 2 Z. J. Lin, F. F. Xie, and G. Z. Su: *J. Surv. Mapp.* **43** (2014) 991. <https://doi.org/10.13485/j.cnki.11-2089.2014.0146>
- 3 X. Y. Zong: *Bull. Surv. Mapp.* **2** (2011) 90 (in Chinese). <https://www.cqvip.com/QK/93318X/20112/36768767.html>

- 4 J. Jia, H. B. Ai, and L. Zhang: Bull. Surv. Mapp. **5** (2013) 62 (in Chinese). <http://qikan.cqvip.com/Qikan/Article/Detail?id=45910073>
- 5 A. P. Chu: Pub. Comm. of Sci. Tech. **10** (2010) 196 (in Chinese). <https://d.wanfangdata.com.cn/periodical/kjcb201020159>
- 6 J. Q. Zhang: Urba. Geo. Inve. Surv. **10** (2013) 73 (in Chinese). <https://doi.org/10.3969/j.issn.1672-8262.2013.05.024>
- 7 Y. J. Yue, D. L. Li, and D. L. Ying: ICMEAS 2010. **01** (2010) 4528. <https://doi.org/10.1109/MACE.2010.5536790>
- 8 C. Y. Zhang, W. Wang, and Y. T. Qiu: Jilin Univ. J. Eng. Technol. Ed. **43** (2013) 1117 (in Chinese). <https://www.cqvip.com/doc/journal/952967513>
- 9 F. F. Xie, Z. J. Lin, and D. Z. Gui: Jilin Univ J. Inf. Sci. Ed. **1** (2014) 56 (in Chinese). <https://doi.org/10.3969/j.issn.1671-5896.2014.01.009>
- 10 Y. F. Li, X. M. Wang, and J. H. Duan: Jilin. Univ. J. Inf. Sci. Ed. **28** (2010) 597 (in Chinese). <https://doi.org/10.3969/j.issn.1671-5896.2010.06.010>
- 11 J. P. Zhou, J. H. Gong, T. Wan, and D. C. Wang: J. Remote Sens. **12** (2008) 877 (in Chinese). <http://qikan.cqvip.com/Qikan/Article/Detail?id=1000948005>
- 12 W. C. Hang: UAV remote sensing image mosaic technology based on POS System. (Nanjing University, Nanjing, 2011).
- 13 D. Turner, A. Lucieer, and C. Watson: Remote Sens. **4** (2012) 1392. <https://doi.org/10.3390/rs4051392>
- 14 H. Lu, Y. S. Li, and J. He: Geo. Inf. Sci. **26** (2010) 16. <https://doi.org/10.1017/S0004972710001772>
- 15 Y. J. Zhang: J. Wuhan. Univ. Inf. Sci. Ed. **34** (2009) 284. <https://www.cqvip.com/doc/journal/991178177>
- 16 Z. Z. Wang: Principles of Photogrammetry. (Surveying and Mapping Publishing Press, Beijing, 1979).
- 17 Z. X. Zhang: Eng. Surv. Mapping. **13** (2004) 1. <https://doi.org/10.3969/j.issn.1006-7949.2004.04.001>
- 18 H. X. Cui, J. Sun, and Z. J. Lin: Sci. Surv. Mapping. **30** (2005) 105. <https://doi.org/10.3771/j.issn.1009-2307.2005.01.035>
- 19 J. Q. Zhang, L. Pan, and S. G. Wang: Photogrammetry (Wuhan University Press, Wuhan, 2003).

About the Authors



Ying Yang received his B.S. degree from Wuhan University, China, in 2007, his M.S. degree from the Chinese Academy of Sciences, China, in 2010, and his Ph.D. degree from Wuhan University, China, in 2017. Since 2017, he has been a senior engineer at the National Basic Geomatics Center of China. His research interests are in photogrammetry, high-performance computing, UAV systems, and sensors. (yangying@ngcc.cn)



Xi Zhai received his B.S. degree in engineering of surveying and mapping from Shandong Agricultural University, China, in 2006 and his M.S. and Ph.D. degrees in cartography and geographical information engineering from Wuhan University, China, in 2012 and 2017, respectively. He has been a senior engineer at the National Geomatics Center of China. His research interests are in emergency mapping, sensor webs, and spatial knowledge services. (zhaixi@ngcc.cn)



Fengzhu Liu received her Ph.D. degree from Wuhan University, China, in 2016. She is working at the Beijing Institute of Survey and Mapping and as a researcher at the Beijing Key Laboratory of Urban Spatial Information Engineering, and since 2018, she has been a senior engineer. Her research interests are in urban 3D spatial data acquisition and processing. (540508818@qq.com)

